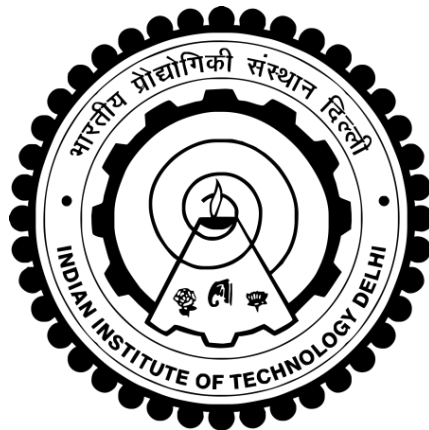


ASSESSMENT AND MITIGATION OF POWER QUALITY DISTURBANCES

RAJ KUMAR



**INSTRUMENT DESIGN DEVELOPMENT CENTRE
INDIAN INSTITUTE OF TECHNOLOGY DELHI
HAUZ KHAS NEW DELHI-110016, INDIA**

OCTOBER 2016

©Indian Institute of Technology Delhi (IITD), New Delhi, 2016

ASSESSMENT AND MITIGATION OF POWER QUALITY DISTURBANCES

by

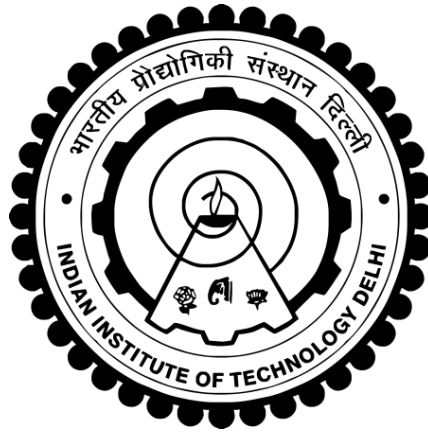
RAJ KUMAR

Instrument Design Development Centre

Submitted

in fulfillment of the requirements of the degree of Doctor of Philosophy

to the



INDIAN INSTITUTE OF TECHNOLOGY DELHI

OCTOBER 2016

CERTIFICATE

It is certified that the thesis entitled “**Assessment and Mitigation of Power Quality Disturbances,**” being submitted by **Mr. Raj Kumar** for award of the degree of **Doctor of Philosophy** in the **Instrument Design Development Centre, Indian Institute of Technology Delhi**, is a record of the student work carried out by him under our supervision and guidance. The matter embodied in this thesis has not been submitted for award of any other degree or diploma.

(Dr. D. T. Shahani)

Professor

**Instrument Design Development Centre
Indian Institute of Technology Delhi
Hauz Khas New Delhi-110016, India**

(Dr. Bhim Singh)

Professor

**Electrical Engineering Department
Indian Institute of Technology Delhi
Hauz Khas New Delhi-110016, India**

Dated:

Place:

ACKNOWLEDGEMENTS

I wish to express my sincere gratitude and indebtedness to **Prof. Bhim Singh** and **Prof. D. T. Shahani** for providing me an opportunity to carry out the Ph.D. work under their supervision. Their keenness and vision have played an important role in guiding me throughout this study. Determination, dedication, innovativeness, resourcefulness and discipline of **Prof. Bhim Singh** and **Prof. D. T. Shahani** have been the inspiration for me to complete this work. Working under them has been a wonderful experience, which has provided a deep insight to the world of research. Their consistent encouragement, continuous monitoring and commitments for excellence have always motivated me to improve my work and use best of my capabilities.

My sincere thanks and deep gratitude to **Prof. Arun Kumar** , **Prof. A. L. Vyas**, **Prof. A. K. Agarwal**, **Prof. G. Bhuvaneswari**, **Prof. S. Mishra** and **Dr. Gufran Sayeed Khan**, all Centre Research Committee members for their valuable guidance and consistent support during the phases of my research work. Thanks are due to Mr. Masood Ali, Mr. Manohar Negi of MDIT Lab. and Sh. Srichand, Sh. Puran Singh of PG Machines Lab. IIT Delhi for providing me the facilities and assistance to carry out experimental work.

I would like to offer my sincere thanks to Dr. Vashist Bist and Mr. Chinmay Jain who helped me a lot to complete my research work. I can not forget the period of my comfortable stay in hostel with Dr. Vashist, Mr. Anup Kumar Mandpura, Mr. Somesh Bhattacharya and Mr. Anshul Varshney during my visits to IIT Delhi and remain supportive and caring throughout my work.

I am also very thankful to Dr. Sabharaj Arya, Dr. Arun Kumar Verma, Dr. Madishetti Sandeep, Dr. N. K. Swami Naidu, Dr. Ram Niwas, Dr. M. Rajesh, Dr. Ujjwal Kalla, Dr. Ashish Srivastava, Mr. Ikhtlaq Hussian, Mr. Rajan Kumar, Mr. Aniket Anand, Mr. Shailendra Dwivedi, Mrs. Geeta Pathak, Mr. Anjanee Kumar Mishra, Mr. Utkarsh Sharma, Mr. Saurav

Shukla, Mr. Sachin Devassy and Mr. Maulik Kandpal for their valuable aid and co-operation and informal support in pursuing experimental work.

I wish to convey my sincere thanks to Prof. V. K. Jain Director SLIET, Longowal for allowing me to pursue Ph.D from IIT Delhi. I also can not forget the support of my friends and colleagues Prof. Ajat Shatru Arora, Dr. Sanjeev Singh, Dr. Ashwani Aggarwal, Mr. Asim Ali Khan, Mr. Parveen Garg, Mr. Jaspal Singh Aujla and Mr. Rakesh Goyal of SLIET, Longowal for their inspiration, support and discussion of my research work .

The completion of this work was not possible without the blessings of my father, Late Sh. Ragho Ram Garg who are not with us to share this joy. The prayers of my mother, Mrs. Shakuntla Devi helped me at every stage of my academic and personal life to see this achievement come true. I must appreciate my wife Mrs. Rimpi Garg for handling the family responsibilities during my stay at IIT Delhi and support to my daughter Bhavika and son Ruhan Garg to see the completion of this work.

I am also grateful to those who have directly or indirectly helped me to complete my thesis work.

Above all, I owe it all to Almighty God for granting me the wisdom, health and strength to undertake this research task and enabling me to its completion.

Dated:

Raj Kumar

ABSTRACT

Power quality problems are arising due to the proliferation of the sensitive electronic loads in industrial and commercial power systems which are the sources of many power quality distortions and disturbances in the distribution system as well as mostly affected by these disturbances. Power quality disturbances generated by these loads propagate on the electrical network to affect the distribution system equipments and causing malfunction of some of the electronic equipments of others. Therefore, due to these power quality issues, the customers are focussing attention on the quality of power necessary for the successful operation of these loads. Ensuring good power quality requires good initial design, effective mitigation equipment, and cooperation with the supplier, frequent monitoring and good maintenance. A high level of power quality is understood as low level of disturbance and agreement on the acceptable levels of disturbance. The limits on power quality are set by certain international standards such as IEEE-1159, IEC 61000 and EN 50160 to maintain the power quality to an acceptable benchmark. When these limits are exceeded, it is not certain that the equipment is no longer to operate or work without any malfunction.

Power quality disturbances like voltage sag, swell, interruption, flicker, notches and spikes commonly occur in a distribution system. Voltage sags are mostly caused by the switching on loads with heavy starting currents and utility fault clearing while the swells are mainly due to the sudden load reduction and a single phase fault on a three phase system. An interruption which is the complete loss of supply voltage is mainly due to any supply grid equipment failure or the operation of the utility protective devices. The flicker which is a symptom of voltage variation is usually caused by large fluctuating loads such as arc furnaces, rolling mill drives and main winders etc. The notching is due to the electronic devices such as variable speed drives, light dimmers and arc welders under normal conditions. The spikes are caused by the lightning, grounding and switching of the inductive

loads. Nonlinear loads are main cause for the origin of the harmonics in the power system. The power system parameters -frequency, voltage and current amplitude, waveform and symmetry can serve as the frames of reference to classify these power quality disturbances according to the impact on the quality of the available power. Disturbances like voltage sag, swell and interruptions are called as events while disturbances like harmonics and flicker are called as power quality variations as these continuously exist in the distribution system. Multistage and multiple power quality disturbances also occur due to the complexity of the power system.

Therefore, the continuous monitoring of power quality is essential today for understanding the causes and the characteristics of various power quality distortions and disturbances so that electrical environment at that location is evaluated to diagnose the incompatibilities between the source and the load. Digital signal processing techniques are used in these instruments for the recognition and the assessment of these power quality disturbances. Power quality disturbances recognition helps the power engineers to solve the power quality issues between the utilities and the consumers and to find the optimum solution for the mitigation of these power quality disturbances. Therefore, the power quality improvements are needed in the form of mitigating devices for the longevity of the electronic equipments. Several measures can be taken at the various levels of the distribution system to make the end use devices less sensitive and to provide the clean and consistent power to the consumers to minimize the equipments failures and operational upsets.

PQ monitoring basically involves the measurements of the voltage and current signals to quantify the performance of the supply, identification of the disturbances and to find the cause of the equipment malfunction. The process of PQ monitoring requires signal processing of the sensed signals for the analysis and the extraction of the relevant features. The main features are extracted from the transformed signals and are used for the classification of these

disturbances so that these techniques can be effectively used for the development of the intelligent PQ monitoring equipments. The selection of the suitable features is extremely important as these features decide the computation time and the precision of the classification. The practical signal processing techniques have been the discrete Fourier transform and the root mean square but these are not suitable for the stationary measurement data. As most of the PQ disturbances are nonstationary in nature so the joint time-frequency domain analysis is needed with the signal processing techniques in order to track the time evolving characteristics of the disturbances.

This research work is aimed towards the development and investigation of signal processing techniques for the assessment and mitigation of various power quality disturbances originating in a distribution system. The simulation to the real acquisition of power quality disturbances are presented in this work. The disturbances are generated in the laboratory by switching a number of linear and nonlinear loads. However, due to the non availability of the practical data and rating constraints, numerical models are used to generate the synthetic data of common power quality disturbances such as voltage sag, swell, interruption, flicker, harmonics, spikes and notches as per IEEE 1159 standard. These are analysed with a number of signal processing techniques like instantaneous symmetrical components, complex wavelet transform, Stockwell-transform, Hilbert Huang transform for the assessment. All the single stage power PQ disturbances are detected and classified using symmetrical components in time domain. The multiple PQ disturbances along with the single stage are detected and assessed with the complex wavelet transform. Stockwell-transform based artificial neural network classifier and rule-based decision tree are proposed for the recognition and the classification of single stage and a number of multiple disturbances. Hilbert Huang transform along with the probabilistic neural network is proposed for the recognition and the classification of the single stage and multiple disturbances.

These signal processing techniques are further investigated for the mitigation of PQ disturbances. Control algorithms based on these techniques for distribution static compensator (DSTATCOM) are proposed for the PQ improvements in a distribution system. A model of a DSTATCOM involving a three leg voltage source converter for a three phase distribution system is developed with the help of Simulink and SimPower toolboxes of MATLAB. The steady state and the dynamic performances are evaluated for both the linear and nonlinear loads under the balanced and unbalanced load conditions simultaneously. The simulated results are validated on a developed laboratory prototype of DSTATCOM. A comparison table of the different algorithms under a nonlinear load in the balanced and unbalanced conditions has been presented. The distortion in the grid current is least at a nonlinear load in the balanced condition with instantaneous symmetrical component technique. The S-transform based control algorithm is providing the least distortion in the grid current during the unbalanced load conditions in the system. PQ indices with these control algorithms are found to within the acceptable limits of international PQ IEEE-519 standard.

TABLE OF CONTENTS

	Page No.
Certificate	i
Acknowledgements	ii
Abstract	iv
Table of Contents	viii
List of Figures	xviii
List of Tables	xxvi
List of Abbreviations	xxvii
List of Symbols	xxix
CHAPTER 1 INTRODUCTION	1-13
1.1 General	1
1.2 State of Art	2
1.2.1 Importance of Power Quality	3
1.2.2 Power Quality Disturbances in Distribution Systems	4
1.2.3 Power Quality Monitoring	5
1.2.4 Power Quality Assessment	6
1.2.5 Power Quality Mitigation in Distribution Systems	7
1.3 Scope of Work	8
1.3.1 Investigations of Signal Processing Techniques for the Detection and Classification of Power Quality Disturbances	8
1.3.2 Analysis, Design and Development of Mitigation Techniques for Power Quality Improvements in Distribution Systems	9
1.3 Outline of Chapters	10
CHAPTER 2 LITERATURE REVIEW	14-32
2.1 General	14
2.2 Literature Survey	14
2.2.1 Definitions of Power Quality	15
2.2.2 Origin of Power Quality Disturbances and Their Consequences	16
2.2.3 Power Quality Standards	19
2.2.4 Power Quality Indices	23

2.2.5	Literature Review of Signal Processing Techniques for Analysis of Power Quality Disturbances	24
2.2.6	Literature Review on Techniques for Classification of Power Quality Disturbances	27
2.2.7	Literature Review on Techniques for Mitigation of Power Quality Disturbances	29
2.3	Identified Research Areas	30
2.4	Conclusions	31

CHAPTER 3 MODELING AND REAL TIME GENERATION OF POWER QUALITY DISTURBANCES 33-51

3.1	General	33
3.2	Classification of Power Quality Disturbances	33
3.3	Analysis and Mathematical Formulation of Power Quality Disturbances	36
3.3.1	Single Stage Power Quality Disturbances	36
3.3.2	Multiple Power Quality Disturbances	37
3.3.3	Multistage Power Quality Disturbances	38
3.4	MATLAB Based Modeling and Simulation of Power Quality Disturbances	39
3.5	Real Time Generation of Power Quality Disturbances	40
3.5.1	Development of Hardware Prototype for Generation of Power Quality Disturbances	40
3.5.2	Development of the Voltage Sensor Board for Power Quality Signal Acquisition	41
3.5.3	Development of the Current Sensor Board for Power Quality Signal Acquisition	42
3.5.4	Power Quality Disturbances Acquisition using LabVIEW-Data Acquisitions Cards (DAQ)	45
3.6	Results and Discussion	45
3.6.1	Simulated Results	46
3.6.2	Experimental Results	46
3.7	Conclusions	50

CHAPTER 4 INSTANTANEOUS SYMMETRICAL COMPONENTS BASED POWER QUALITY ASSESSMENT 52-70

4.1	General	52
4.2	Theory of Instantaneous Symmetrical Components in Time Domain	52

4.3	Modeling and Simulation of Power Quality Disturbances Detection	54
4.4	Feature Extraction and Method for Power Quality Disturbances Classification	55
4.5	Hardware Implementation of Power Quality Disturbances Detection	59
4.6	Results and Discussion	60
4.6.1	Simulation Results	60
4.6.1.1	Detection of Voltage Sag	60
4.6.1.2	Detection of Voltage Swell	61
4.6.1.3	Detection of Voltage Flicker	62
4.6.1.4	Detection of Voltage Harmonics	62
4.6.1.5	Detection of Voltage Notches	63
4.6.1.6	Detection of Voltage Oscillatory Transients	63
4.6.1.7	Detection of Voltage Spike	65
4.6.1.8	Detection of Voltage Interruption	65
4.6.2	Experimental Results	66
4.6.2.1	Detection of Real Time Voltage Sag	66
4.6.2.2	Detection of Real Time Voltage Swell	67
4.6.2.3	Detection of Real Time Voltage Notch	67
4.6.2.4	Detection of Real Time Voltage Interruption	67
4.6.3	Classification of Power Quality Disturbances	69
4.7	Conclusions	70

CHAPTER 5 COMPLEX WAVELET BASED POWER QUALITY ASSESSMENT 71-92

5.1	General	71
5.2	Theory of Complex Wavelet-Multiresolution Signal Decomposition	71
5.3	Modeling and Simulation of Power Quality Disturbances Detection	73
5.4	Feature Extraction and Method for Power Quality Disturbances Classification	74
5.5	Hardware Implementation of Power Quality Disturbances Detection	76
5.6	Results and Discussion	77
5.6.1	Simulation Results	77
5.6.1.1	Detection of Voltage Sag	77
5.6.1.2	Detection of Voltage Swell	78
5.6.1.3	Detection of Voltage Flicker	78
5.6.1.4	Detection of Voltage Harmonics	80
5.6.1.5	Detection of Voltage Notches	80

5.6.1.6	Detection of Voltage Oscillatory Transients	81
5.6.1.7	Detection of Voltage Spike	81
5.6.1.8	Detection of Voltage Interruption	83
5.6.1.9	Detection of Voltage Sag with Harmonics	83
5.6.1.10	Detection of Voltage Swell with Harmonics	84
5.6.1.11	Detection of Voltage Flicker with Harmonics	84
5.6.2	Experimental Results	86
5.6.2.1	Detection of Real Time Voltage Sag	86
5.6.2.2	Detection of Real Time Voltage Swell	87
5.6.2.3	Detection of Real Time Voltage Notch	88
5.6.2.4	Detection of Real Time Voltage Oscillatory Transient	89
5.6.3	Classification of Power Quality Disturbances	90
5.7	Conclusions	91

CHAPTER 6 STOCKWELL TRANSFORM BASED POWER QUALITY ASSESSMENT 93-114

6.1	General	93
6.2	Theory of Stockwell-Transform	93
6.3	Modeling and Simulation of Power Quality Disturbances Detection	96
6.4	Feature Extraction and Method for Power Quality Disturbances Classification	97
6.4.1	Rule Based Decision Tree	97
6.4.2	Artificial Neural Network	98
6.5	Hardware Implementation of Power Quality Disturbances Detection	100
6.6	Results and Discussion	101
6.6.1	Simulation Results	101
6.6.1.1	Detection of Voltage Sag	101
6.6.1.2	Detection of Voltage Swell	101
6.6.1.3	Detection of Voltage Flicker	102
6.6.1.4	Detection of Voltage Harmonics	103
6.6.1.5	Detection of Voltage Notches	103
6.6.1.6	Detection of Voltage Oscillatory Transients	104
6.6.1.7	Detection of Voltage Spike	105
6.6.1.8	Detection of Voltage Interruption	105
6.6.1.9	Detection of Voltage Sag with Harmonics	106
6.6.1.10	Detection of Voltage Swell with Harmonics	107

6.6.1.11	Detection of Voltage Flicker with Harmonics	108
6.6.2	Experimental Results	108
6.6.2.1	Detection of Real Time Voltage Sag	108
6.6.2.2	Detection of Real Time Voltage Swell	109
6.6.2.3	Detection of Real Time Voltage Notch	110
6.6.2.4	Detection of Real Time Voltage Oscillatory Transient	111
6.6.3	Classification of Power Quality Disturbances using Rule-Based Decision Tree and Artificial Neural Network	112
6.7	Conclusions	114

CHAPTER 7 HILBERT HUANG TRANSFORM BASED POWER QUALITY ASSESSMENT 115-141

7.1	General	115
7.2	Theory of Hilbert Huang Transform	115
7.2.1	Empirical Mode Decomposition	115
7.2.2	Hilbert Transform	116
7.3	Modeling and Simulation of Power Quality Disturbances Detection	118
7.4	Feature Extraction for Power Quality Disturbances Classification	118
7.5	Hardware Implementation of Power Quality Disturbances Detection	120
7.6	Results and Discussion	121
7.6.1	Simulation Results	121
7.6.1.1	Detection of Voltage Sag	122
7.6.1.2	Detection of Voltage Swell	122
7.6.1.3	Detection of Voltage Flicker	123
7.6.1.4	Detection of Voltage Harmonics	123
7.6.1.5	Detection of Voltage Notches	125
7.6.1.6	Detection of Voltage Oscillatory Transients	125
7.6.1.7	Detection of Voltage Spikes	126
7.6.1.8	Detection of Voltage Interruption	127
7.6.1.9	Detection of Voltage Flicker with Sag	127
7.6.1.10	Detection of Voltage Flicker with Swell	128
7.6.1.11	Detection of Voltage Sag with Harmonics	128
7.6.1.12	Detection of Voltage Swell with Harmonics	130
7.6.1.13	Detection of Voltage Harmonics with Sag	130
7.6.1.14	Detection of Voltage Harmonics with Swell	131
7.6.1.15	Detection of Voltage Transients with Harmonics	132

7.6.1.16	Detection of Voltage Transients with Sag	132
7.6.1.17	Detection of Voltage Transients with Swell	133
7.6.2	Experimental Results	134
7.6.2.1	Detection of Real Time Voltage Sag	135
7.6.2.2	Detection of Real Time Voltage Swell	136
7.6.2.3	Detection of Real Time Voltage Notch	137
7.6.2.4	Detection of Real Time Voltage Oscillatory Transient	137
7.6.3	Classification of Power Quality Disturbances using Probabilistic Neural Network	138
7.7	Conclusions	140
CHAPTER 8	INSTANTANEOUS SYMMETRICAL COMPONENTS THEORY BASED CONTROL ALGORITHM OF DSTATCOM FOR POWER QUALITY IMPROVEMENT	142-163
8.1	General	142
8.2	System Configuration of Distribution Static Compensator (DSTATCOM)	142
8.3	Control Algorithm Based on Instantaneous Symmetrical Components Theory	146
8.3.1	Estimation of Average Active Power	147
8.3.2	Estimation of Reference Currents	148
8.4	Modeling and Simulation of Instantaneous Symmetrical Components Based Control Algorithm of DSTATCOM	148
8.5	Hardware Implementation of Instantaneous Symmetrical Components Based Control Algorithm of DSTATCOM	149
8.6	Results and Discussion	151
8.6.1	Simulated Performance	151
8.6.1.1	Intermediate Signals of Instantaneous Symmetrical Components Based Control Algorithm	151
8.6.1.2	System Performance under Balanced and Unbalanced Linear Loads	152
8.6.1.3	System Performance under Balanced and Unbalanced Nonlinear Loads	153
8.6.2	Experimental Performance	155
8.6.2.1	Intermediate Signals of Instantaneous Symmetrical Components Based Control Algorithm	155
8.6.2.2	Steady State Performance	156
8.6.2.2.1	Steady State Performance under Linear Load	156

	8.6.2.2.2	Steady State Performance under Nonlinear Load	157
	8.6.2.3	Dynamic Performance	159
	8.6.2.3.1	Dynamic Performance under Linear Unbalanced Load	160
	8.6.2.3.2	Dynamic Performance under Nonlinear Unbalanced Load	161
8.7		Conclusions	163
CHAPTER 9		S-TRANSFORM BASED CONTROL ALGORITHM OF DSTATCOM FOR POWER QUALITY IMPROVEMENT	164-186
9.1		General	164
9.2		System Configuration of Distribution Static Compensator (DSTATCOM)	164
9.3		Control algorithm Based on S-Transform	165
	9.3.1	Estimation of the PCC Voltages Unit Templates	166
	9.3.2	Estimation of the Net Active Power Component	167
	9.3.3	Estimation of the References Supply Currents	169
	9.3.4	Generation of the Switching Pulses of VSC	169
9.4		Modeling and Simulation of S-Transform Based Control Algorithm of DSTATCOM	169
9.5		Hardware Implementation of S-Transform Based Control Algorithm of DSTATCOM	172
9.6		Results and Discussion	172
	9.6.1	Simulated Performance	172
	9.6.1.1	Intermediate Signals of S-Transform Based Control Algorithm	172
	9.6.1.2	System Performance under Balanced and Unbalanced Linear Loads	174
	9.6.1.3	System Performance under Balanced and Unbalanced Nonlinear Loads	175
	9.6.2	Experimental Performance	176
	9.6.2.1	Intermediate Signals of S-Transform Based Control Algorithm	176
	9.6.2.2	Steady State Performance	178
	9.6.2.2.1	Steady State Performance under Linear Load	178
	9.6.2.2.2	Steady State Performance under Nonlinear Load	179

9.6.2.3	Dynamic Performance	180
9.6.2.3.1	Dynamic Performance under Linear Unbalanced Load	182
9.6.2.3.2	Dynamic Performance under Nonlinear Unbalanced Load	184
9.7	Conclusions	185
CHAPTER 10	COMPLEX WAVELET TRANSFORM BASED CONTROL ALGORITHM OF DSTATCOM FOR POWER QUALITY IMPROVEMENT	187-209
10.1	General	187
10.2	System Configuration of Distribution Static Compensator (DSTATCOM)	187
10.3	Control Algorithm Based on Complex Wavelet Transform	189
10.3.1	Estimation of the PCC Voltages Unit Templates	190
10.3.2	Estimation of the Average Active Power Components of Load Currents	190
10.3.3	Estimation of the Active Power Component of DC Link Voltage Control	192
10.3.4	Estimation of the Net Active Power Component	192
10.3.5	Estimation of References Currents	192
10.3.6	Generation of Switching Pulses of VSC	193
10.4	Modeling and Simulation of Complex Wavelet Transform Based Control Algorithm of DSTATCOM	193
10.5	Hardware Implementation of Complex Wavelet Transform Based Control Algorithm of DSTATCOM	196
10.6	Results and Discussion	196
10.6.1	Simulated Performance	196
10.6.1.1	Intermediate Signals of Complex Wavelet Transform Based Control Algorithm	196
10.6.1.2	System Performance under Balanced and Unbalanced Linear Loads	199
10.6.1.3	System Performance under Balanced and Unbalanced Nonlinear Loads	199
10.6.2	Experimental Performance	200
10.6.2.1	Intermediate Signals of Complex Wavelet Transform Based Control Algorithm	202

10.6.2.2	Steady State Performance	202
10.6.2.2.1	Steady State Performance under Linear Load	203
10.6.2.2.2	Steady State Performance under Nonlinear Load	204
10.6.2.3	Dynamic Performance	206
10.6.2.3.1	Dynamic Performance under Linear Unbalanced Load	206
10.6.2.3.2	Dynamic Performance under Nonlinear Unbalanced Load	207
10.7	Conclusions	209

CHAPTER 11 HILBERT HUANG TRANSFORM BASED CONTROL ALGORITHM OF DSTATCOM FOR POWER QUALITY IMPROVEMENT 210-230

11.1	General	210
11.2	System Configuration of Distribution Static Compensator (DSTATCOM)	210
11.3	Control Algorithm Based on Hilbert Huang Transform	211
11.3.1	Estimation of in-Phase and Quadrature Unit Templates of PCC Voltages	212
11.3.2	Estimation of the Average Active Power Components of Load Currents	213
11.3.3	Estimation of Net Active Power Component of the Grid Current	213
11.3.4	Estimation of References Source Currents	213
11.3.5	Estimation of Gating Pulses of VSC	214
11.4	Modeling and Simulation of Hilbert Huang Transform Based Control Algorithm of DSTATCOM	214
11.5	Hardware Implementation of Hilbert Huang Transform Based Control Algorithm of DSTATCOM	217
11.6	Results and Discussion	217
11.6.1	Simulated Performance	217
11.6.1.1	Intermediate Signals of Hilbert Huang Transform Based Control Algorithm	218
11.6.1.2	System Performance under Balanced and Unbalanced Linear Loads	219
11.6.1.3	System Performance under Balanced and Unbalanced Nonlinear Loads	220
11.6.2	Experimental Performance	222

11.6.2.1	Intermediate Signals of Hilbert Huang Transform Based Control Algorithm	222
11.6.2.2	Steady State Performance	223
11.6.2.2.1	Steady State Performance under Linear Load	223
11.6.2.2.2	Steady State Performance under Nonlinear Load	225
11.6.2.3	Dynamic Performance	225
11.6.2.3.1	Dynamic Performance under Linear Unbalanced Load	227
11.6.2.3.2	Dynamic Performance under Nonlinear Unbalanced Load	229
11.7	Conclusions	230
CHAPTER 12	MAIN CONCLUSIONS AND SUGGESTIONS FOR FURTHER WORK	231-238
12.1	General	231
12.2	Main Conclusions	232
12.3	Suggestions for Further Work	237
REFERENCES		239-246
APPENDICES		247-251
LIST OF PUBLICATIONS		252
BIO-DATA		253

LIST OF FIGURES

- Fig. 1.1 General scheme of PQ monitoring
- Fig. 2.1 CBEMA curve
- Fig. 3.1 Prototype of the developed hardware for real-time PQ disturbances generation and Acquisition
- Fig. 3.2 Actual system for the acquisition of the PQ disturbances
- Fig. 3.3 Interfacing circuit of voltage sensing and signal conditioning circuit
- Fig. 3.4 PCB developed in laboratory for voltage sensing and signal conditioning circuit
- Fig. 3.5 Schematic diagram of current sensing circuitry
- Fig. 3.6 PCB developed in laboratory for current sensing and signal conditioning circuit
- Fig. 3.7 Simulated disturbances as (a) sag (b) swell (c) harmonic (d) flicker (e) notch (f) oscillatory transient (g) spike (h) interruption (i) osc. transient with sag (j) sag with harmonic
- Fig. 3.8 (a) Digital storage Oscilloscope image of transient signal and (b) Real time transient signal generated by capacitor switching
- Fig. 3.9 (a) Digital storage Oscilloscope image of voltage notch signal and (b) Real time voltage notch signal generated by a three phase rectifier
- Fig. 3.10 (a) Digital storage Oscilloscope image of voltage sag signal and (b) Real time voltage sag signal generated by switching a high rating load
- Fig. 3.11 (a) Digital storage Oscilloscope image of voltage swell signal and (b) Real time voltage swell signal generated by removing a high rating load
- Fig. 4.1 Block diagram of a PLL
- Fig. 4.2 Schematic of the PQ disturbance detection
- Fig. 4.3 Block scheme for the classification of single stage PQ disturbances
- Fig. 4.4 A prototype of developed hardware for real-time PQ disturbance generation and detection
- Fig. 4.5 (a) Voltage sag (b) Negative sequence component of disturbance phase, Instantaneous Peak value contour calculated from the (c) positive and (d) negative sequence components
- Fig. 4.6 (a) Voltage Swell (b) Negative sequence component of disturbance phase, Instantaneous Peak value contour calculated from the (c) positive and (d) negative sequence components
- Fig. 4.7 (a) Voltage flicker (b) Negative sequence component of disturbance phase, Instantaneous Peak value contour calculated from the (c) positive and (d) negative sequence components
- Fig. 4.8 (a) Voltage harmonics (b) Negative sequence component of disturbance phase, Instantaneous Peak value contour calculated from the (c) positive and (d) negative sequence components
- Fig. 4.9 (a) Voltage notch (b) Negative sequence component of disturbance phase, Instantaneous Peak value contour calculated from the (c) positive and (d) negative sequence components
- Fig. 4.10 (a) Voltage oscillatory transient (b) Negative sequence component of disturbance phase, Instantaneous Peak value contour calculated from the (c) positive and (d) negative sequence components
- Fig.4.11 (a) Voltage spike (b) Negative sequence component of disturbance phase,

- Instantaneous Peak value contour calculated from the (c) positive and (d) negative sequence components
- Fig.4.12 (a) Voltage interruption (b) Negative sequence component of disturbance phase, Instantaneous Peak value contour calculated from the (c) positive and (d) negative sequence components
- Fig. 4.13 (a) Real time voltage sag (b) Negative sequence component of disturbance phase, Instantaneous Peak value contour calculated from the (c) positive and (d) negative sequence components
- Fig. 4.14 (a) Real time voltage swell (b) Negative sequence component of disturbance phase, Instantaneous Peak value contour calculated from the (c) positive and (d) negative sequence components
- Fig. 4.15 (a) Real time voltage notch (b) Negative sequence component of disturbance phase, Instantaneous Peak value contour calculated from the (c) positive and (d) negative sequence components
- Fig. 4.16 (a) Real time voltage interruption (b) Negative sequence component of disturbance phase, Instantaneous Peak value contour calculated from the (c) positive and (d) negative sequence components
- Fig. 5.1 Analysis filter bank for DT-DWT based CWT
- Fig. 5.2 Block scheme for the classification of single stage PQ disturbances
- Fig. 5.3 CWT decomposition of the voltage sag signal
- Fig. 5.4 CWT decomposition of the voltage swell signal
- Fig. 5.5 CWT decomposition of the voltage flicker signal
- Fig. 5.6 CWT decomposition of the voltage harmonics signal
- Fig. 5.7 CWT decomposition of the voltage notch signal
- Fig. 5.8 CWT decomposition of voltage oscillatory transient signal
- Fig. 5.9 CWT decomposition of the voltage spike signal
- Fig. 5.10 CWT decomposition of the voltage interruption signal
- Fig. 5.11 CWT decomposition of the voltage sag with harmonics signal
- Fig. 5.12 CWT decomposition of the voltage swell with harmonics signal
- Fig. 5.13 CWT decomposition of the voltage flicker with harmonics signal
- Fig. 5.14 (a) A real time voltage sag disturbance (b) CWT decomposition of the real time sag signal
- Fig. 5.15 (a) A real time voltage swell disturbance (b) CWT decomposition of the real time swell signal
- Fig. 5.16 (a) A real time voltage notch disturbance (b) CWT decomposition of the real time notch signal
- Fig. 5.17 (a) A real time voltage osc. transient disturbance (b) CWT decomposition of the real time transient signal
- Fig. 6.1 Block scheme for the classifications of single and multistage PQ disturbances
- Fig. 6.2 (a) Detection of voltage sag (b) Maximum amplitude versus time contour (c) Amplitude versus frequency (normalized) contour
- Fig. 6.3 (a) Detection of voltage swell (b) Maximum amplitude versus time contour (c) Amplitude versus frequency (normalized) contour
- Fig. 6.4 (a) Detection of voltage flicker (b) Maximum amplitude versus time contour (c) Amplitude versus frequency (normalized) contour
- Fig. 6.5 (a) Detection of voltage harmonics (b) Maximum amplitude versus time contour

- (c) Amplitude versus frequency (normalized) contour
- Fig. 6.6 (a) Detection of voltage notches (b) Maximum amplitude versus time contour (c) Amplitude versus frequency (normalized) contour
- Fig. 6.7 (a) Detection of voltage oscillatory transient (b) Maximum amplitude versus time contour (c) Amplitude versus frequency (normalized) contour
- Fig. 6.8 (a) Detection of voltage spikes (b) Maximum amplitude versus time contour (c) Amplitude versus frequency (normalized) contour
- Fig. 6.9 (a) Detection of voltage interruption (b) Maximum amplitude versus time contour (c) Amplitude versus frequency (normalized) contour
- Fig. 6.10 (a) Detection of voltage sag with harmonics (b) Maximum amplitude versus time contour (c) Amplitude versus frequency (normalized) contour
- Fig. 6.11 (a) Detection of voltage swell with harmonics (b) Maximum amplitude versus time contour (c) Amplitude versus frequency (normalized) contour
- Fig. 6.12 (a) Detection of voltage flicker with harmonics (b) Maximum amplitude versus time contour (c) Amplitude versus frequency (normalized) contour
- Fig. 6.13 (a) Generation of real-time voltage sag signal and its (b) S-transform analysis
- Fig. 6.14 (a) Generation of real-time voltage swell signal and its (b) S-transform analysis
- Fig. 6.15 (a) Generation of real-time voltage notch signal and its (b) S-transform analysis
- Fig. 6.16 (a) Generation of real-time voltage transient signal and its (b) S-transform analysis
- Fig. 7.1 Probabilistic neural network
- Fig. 7.2 Voltage sag and its corresponding first three intrinsic mode functions (A1-A3), its instantaneous amplitude (B1-B3), instantaneous phase (C1-C3) and its instantaneous frequency (D1-D3)
- Fig. 7.3 Voltage swell and its corresponding first three intrinsic mode functions (A1-A3), its instantaneous amplitude (B1-B3), instantaneous phase (C1-C3) and its instantaneous frequency (D1-D3)
- Fig. 7.4 Voltage flicker and its corresponding first three intrinsic mode functions (A1-A3), its instantaneous amplitude (B1-B3), instantaneous phase (C1-C3) and its instantaneous frequency (D1-D3)
- Fig. 7.5 Voltage harmonics and its corresponding first three intrinsic mode functions (A1-A3), its instantaneous amplitude (B1-B3), instantaneous phase (C1-C3) and its instantaneous frequency (D1-D3)
- Fig. 7.6 Voltage notches and its corresponding first three intrinsic mode functions (A1-A3), its instantaneous amplitude (B1-B3), instantaneous phase (C1-C3) and its instantaneous frequency (D1-D3)
- Fig. 7.7 Voltage oscillatory transient and its corresponding first three intrinsic mode functions (A1-A3), its instantaneous amplitude (B1-B3), instantaneous phase (C1-C3) and its instantaneous frequency (D1-D3)
- Fig. 7.8 Voltage spikes and its corresponding first three intrinsic mode functions (A1-A3), its instantaneous amplitude (B1-B3), instantaneous phase (C1-C3) and its instantaneous frequency (D1-D3)
- Fig. 7.9 Voltage interruption and its corresponding first three intrinsic mode functions (A1-A3), its instantaneous amplitude (B1-B3), instantaneous phase (C1-C3) and its instantaneous frequency (D1-D3)
- Fig. 7.10 Voltage flicker with sag and its corresponding first three intrinsic mode functions (A1-A3), its instantaneous amplitude (B1-B3), instantaneous phase (C1-C3) and its instantaneous frequency (D1-D3)

- Fig. 7.11 Voltage flicker with swell and its corresponding first three intrinsic mode functions (A1-A3), its instantaneous amplitude (B1-B3), instantaneous phase (C1-C3) and its instantaneous frequency (D1-D3)
- Fig. 7.12 Voltage sag with harmonic and its corresponding first three intrinsic mode functions (A1-A3), its instantaneous amplitude (B1-B3), instantaneous phase (C1-C3) and its instantaneous frequency (D1-D3)
- Fig. 7.13 Voltage swell with harmonic and its corresponding first three intrinsic mode functions (A1-A3), its instantaneous amplitude (B1-B3), instantaneous phase (C1-C3) and its instantaneous frequency (D1-D3)
- Fig. 7.14 Voltage harmonic with sag and its corresponding first three intrinsic mode functions (A1-A3), its instantaneous amplitude (B1-B3), instantaneous phase (C1-C3) and its instantaneous frequency (D1-D3)
- Fig. 7.15 Voltage harmonic with swell and its corresponding first three intrinsic mode functions (A1-A3), its instantaneous amplitude (B1-B3), instantaneous phase (C1-C3) and its instantaneous frequency (D1-D3)
- Fig. 7.16 Voltage transient with harmonics and its corresponding first three intrinsic mode functions (A1- A3), its instantaneous amplitude (B1-B3), instantaneous phase (C1-C3) and its instantaneous frequency (D1-D3)
- Fig. 7.17 Voltage transient with sag and its corresponding first three intrinsic mode functions (A1- A3), its instantaneous amplitude (B1-B3), instantaneous phase (C1-C3) and its instantaneous frequency (D1-D3)
- Fig. 7.18 Voltage transient with swell and its corresponding first three intrinsic mode functions (A1- A3), its instantaneous amplitude (B1-B3), instantaneous phase (C1-C3) and its instantaneous frequency (D1-D3)
- Fig. 7.19 (a) Generation of real-time voltage sag signal and its (b) first three intrinsic mode functions (A1- A3), its instantaneous amplitude (B1-B3), instantaneous phase (C1-C3) and its instantaneous frequency (D1-D3)
- Fig. 7.20 (a) Generation of real-time voltage swell signal and its (b) first three intrinsic mode functions (A1- A3), its instantaneous amplitude (B1-B3), instantaneous phase (C1-C3) and its instantaneous frequency (D1-D3)
- Fig. 7.21 (a) Generation of real-time voltage notch signal and its (b) first three intrinsic mode functions (A1- A3), its instantaneous amplitude (B1-B3), instantaneous phase (C1-C3) and its instantaneous frequency (D1-D3)
- Fig. 7.22 (a) Generation of real-time voltage oscillatory transient signal and its (b)) first three intrinsic mode functions (A1- A3), its instantaneous amplitude (B1-B3), instantaneous phase (C1-C3) and its instantaneous frequency (D1-D3)
- Fig. 8.1 Schematic of a DSTATCOM
- Fig. 8.2 Instantaneous symmetrical component theory based control algorithm of VSC
- Fig. 8.3 MATLAB model of DSTATCOM using Instantaneous symmetrical component theory based control algorithm
- Fig. 8.4 Instantaneous symmetrical component theory based control algorithm (a) estimation of the PCC voltage unit templates (b) reference current estimation
- Fig. 8.5 Prototype of the developed hardware of DSTATCOM
- Fig. 8.6 Intermediate signals of the Instantaneous Symmetrical Components Based Control Algorithm for a nonlinear load with unbalancing in 'c' phase
- Fig. 8.7 System behaviour under balanced linear load with unbalancing from time $t=0.4$ s to 0.5 s
- Fig. 8.8 System behaviour under balanced nonlinear load with unbalancing from time $t=0.4$ s to 0.5 s

- Fig. 8.9 Harmonic spectra of the proposed system at balanced load condition (a) v_{sab} (b) i_{sa} (c) i_{La}
- Fig. 8.10 Harmonic spectra of the proposed system at unbalanced load condition (a) v_{sab} (b) i_{sa} (c) i_{La}
- Fig. 8.11 Salient internal signals of the control algorithm during the nonlinear load disconnection (a) i_{Lc} , p_s , p_{st} and p_{loss} (b) D , P_{st}/D , i_{cref} and i_{sc}
- Fig. 8.12 Salient internal signals of the control algorithm during the nonlinear load injection (a) i_{Lc} , p_s , p_{st} and p_{loss} (b) D , P_{st}/D , i_{cref} and i_{sc}
- Fig. 8.13 DSTATCOM performance under linear balanced load (a) Grid power (b) Load power (c) Compensating power
- Fig. 8.14 DSTATCOM performance under linear unbalanced load (a)-(c) grid currents i_{sa} , i_{sb} , i_{sc} with grid voltage v_{sab} (d)-(f) load currents i_{La} , i_{Lb} , i_{Lc} with grid voltage v_{sab} (g)-(i) compensating currents i_{sa} , i_{sb} , i_{sc} with grid voltage v_{sab}
- Fig. 8.15 DSTATCOM performance under nonlinear balanced load (a)-(c) grid currents i_{sa} , i_{sb} , i_{sc} with grid voltage v_{sab} (d)-(f) THD's of i_{sa} , i_{sb} , i_{sc} (g)-(i) load currents i_{La} , i_{Lb} , i_{Lc} with grid voltage v_{sab} (j)-(l) THD's of i_{La} , i_{Lb} , i_{Lc} (m)-(o) compensating currents i_{sa} , i_{sb} , i_{sc} along with voltage v_{sab} (p)-(r) grid power, load power and compensating power
- Fig. 8.16 DSTATCOM performance under nonlinear unbalanced load (a)-(c) grid currents i_{sa} , i_{sb} , i_{sc} along with grid voltage v_{sab} (d)-(f) load currents i_{La} , i_{Lb} , i_{Lc} with grid voltage v_{sab} (g)-(i) compensating currents i_{sa} , i_{sb} , i_{sc} with grid voltage v_{sab}
- Fig. 8.17 DSTATCOM performance during the linear load disconnection in phase 'c' (a) v_{sab} , i_{sa} , i_{sb} and i_{sc} (b) v_{sab} , i_{La} , i_{Lb} and i_{Lc} (c) v_{sab} , i_{ca} , i_{cb} and i_{cc} (d) V_{dc} , i_{sc} , i_{Lc} and i_{cc}
- Fig. 8.18 DSTATCOM performance during the linear load injection in phase 'c' (a) v_{sab} , i_{sa} , i_{sb} and i_{sc} (b) v_{sab} , i_{La} , i_{Lb} and i_{Lc} (c) v_{sab} , i_{ca} , i_{cb} and i_{cc} (d) V_{dc} , i_{sc} , i_{Lc} and i_{cc}
- Fig. 8.19 DSTATCOM performance during the nonlinear load disconnection in phase 'c' (a) v_{sab} , i_{sa} , i_{sb} and i_{sc} (b) v_{sab} , i_{La} , i_{Lb} and i_{Lc} (c) v_{sab} , i_{ca} , i_{cb} and i_{cc} (d) V_{dc} , i_{sc} , i_{Lc} and i_{cc}
- Fig. 8.20 DSTATCOM performance during the nonlinear load injection in phase 'c' (a) v_{sab} , i_{sa} , i_{sb} and i_{sc} (b) v_{sab} , i_{La} , i_{Lb} and i_{Lc} (c) v_{sab} , i_{ca} , i_{cb} and i_{cc} (d) V_{dc} , i_{sc} , i_{Lc} and i_{cc}
- Fig. 9.1 Schematic of a DSTATCOM
- Fig. 9.2 Block diagram of S-transform based control algorithm for a DSTATCOM
- Fig. 9.3 MATLAB model of DSTATCOM using S-transform based control algorithm
- Fig. 9.4 S-transform theory based control algorithm of DSTATCOM (a) extraction of fundamental component of load current (b) extraction of the active component of load current (c) extraction of average active component of load current (d) unit templates estimation (e) generation of gate signals
- Fig. 9.5 Harmonic components of the 'c' phase load current
- Fig. 9.6 Intermediate signals of the S-transform based control algorithm for a nonlinear load with unbalancing in 'c' phase
- Fig. 9.7 System behaviour under balanced linear load with unbalancing from time $t=0.4$ s to 0.5 s
- Fig. 9.8 System behaviour under balanced nonlinear load with unbalancing from time $t=0.4$ s to 0.5 s
- Fig. 9.9 Harmonic spectra of the proposed system at balanced load condition (a) v_{sab} (b) i_{sa} (c) i_{La}
- Fig. 9.10 Harmonic spectra of the proposed system at unbalanced load condition (a) v_{sab} (b) i_{sa} (c) i_{La}
- Fig. 9.11 Salient internal signals of the control algorithm (a) i_{Lc} , i_{fLc} , i_{AfLc} and $abs(i_{AfLc})$

- (b) i_{Lc} , I_{ApLg} , I_{nApLg} and I_{pdc} (c) i_{Lc} , u_{cp} , i_{cref} and i_{sc}
- Fig. 9.12 DSTATCOM performance under linear balanced load (a) Grid power (b) Load power (c) Compensating power
- Fig. 9.13 DSTATCOM performance under linear unbalanced load (a)-(c) grid currents i_{sa} , i_{sb} , i_{sc} with grid voltage v_{sab} (d)-(f) load currents i_{La} , i_{Lb} , i_{Lc} with grid voltage v_{sab} (g)-(i) compensating currents i_{sa} , i_{sb} , i_{sc} with grid voltage v_{sab}
- Fig. 9.14 DSTATCOM performance under nonlinear balanced load (a)-(c) grid currents i_{sa} , i_{sb} , i_{sc} with grid voltage v_{sab} (d)-(f) THD's of i_{sa} , i_{sb} , i_{sc} (g)-(i) load currents i_{La} , i_{Lb} , i_{Lc} with grid voltage v_{sab} (j)-(l) THD's of i_{La} , i_{Lb} , i_{Lc} (m)-(o) compensating currents i_{sa} , i_{sb} , i_{sc} along with voltage v_{sab} (p)-(r) grid power, load power and compensating power
- Fig. 9.15 DSTATCOM performance under nonlinear unbalanced load (a)-(c) grid currents i_{sa} , i_{sb} , i_{sc} along with grid voltage v_{sab} (d)-(f) load currents i_{La} , i_{Lb} , i_{Lc} with grid voltage v_{sab} (g)-(i) compensating currents i_{sa} , i_{sb} , i_{sc} with grid voltage v_{sab}
- Fig. 9.16 DSTATCOM performance during the linear load disconnection in phase 'c' (a) v_{sab} , i_{sa} , i_{sb} and i_{sc} (b) v_{sab} , i_{La} , i_{Lb} and i_{Lc} (c) v_{sab} , i_{ca} , i_{cb} and i_{cc} (d) V_{dc} , i_{sc} , i_{Lc} and i_{cc}
- Fig. 9.17 DSTATCOM performance during the linear load injection in phase 'c' (a) v_{sab} , i_{sa} , i_{sb} and i_{sc} (b) v_{sab} , i_{La} , i_{Lb} and i_{Lc} (c) v_{sab} , i_{ca} , i_{cb} and i_{cc} (d) V_{dc} , i_{sc} , i_{Lc} and i_{cc}
- Fig. 9.18 DSTATCOM performance during the nonlinear load disconnection in phase 'c' (a) v_{sab} , i_{sa} , i_{sb} and i_{sc} (b) v_{sab} , i_{La} , i_{Lb} and i_{Lc} (c) v_{sab} , i_{ca} , i_{cb} and i_{cc} (d) V_{dc} , i_{sc} , i_{Lc} and i_{cc}
- Fig. 9.19 DSTATCOM performance during the nonlinear load injection in phase 'c' (a) v_{sab} , i_{sa} , i_{sb} and i_{sc} (b) v_{sab} , i_{La} , i_{Lb} and i_{Lc} (c) v_{sab} , i_{ca} , i_{cb} and i_{cc} (d) V_{dc} , i_{sc} , i_{Lc} and i_{cc}
- Fig. 10.1 Schematic of a DSTATCOM
- Fig. 10.2. Block diagram of DT-CWT based control algorithm for a DSTATCOM
- Fig. 10.3 DT-CWT decomposition of load current signal
- Fig. 10.4 MATLAB model of DSTATCOM using DT-DWT based control algorithm
- Fig. 10.5 DT-DWT based control algorithm of DSTATCOM (a) extraction of PCC voltage unit templates (b) estimation of the fundamental component of 'c' phase load current (b) estimation of the active component of load current (d) extraction of average active component of load current (e) reference current estimation (f) generation of gate signals
- Fig. 10.6 Coefficients of imaginary tree of the 'c' phase load current
- Fig. 10.7 Harmonic estimation of the CWT levels of 'c' phase load current (a) I_{Lc} (a) I_{Lc2} (a) I_{Lc4}
- Fig. 10.8 Intermediate signals of the CWT based control algorithm for a nonlinear load with unbalancing in 'c' phase
- Fig. 10.9 System behaviour under balanced linear load with unbalancing from time t=0.4 s to 0.5 s
- Fig. 10.10 System behaviour under balanced nonlinear load with unbalancing from time t = 0.4 s to 0.5 s
- Fig. 10.11 Harmonic spectra of the proposed system at balanced load condition (a) v_{sab} (b) i_{sa} (c) i_{La}
- Fig. 10.12 Harmonic spectra of the proposed system at unbalanced load condition (a) v_{sab} (b) i_{sa} (c) i_{La}
- Fig. 10.13 Salient internal signals of the control algorithm (a) i_{Lc} , i_{qfLc} , u_{cp} and $\text{abs}(i_{AfLc})$ (b) i_{Lc} , I_{ApLg} , $\text{abs}(I_{pdc})$ and I_{nApLg} (c) i_{Lc} , I_{nApLg} , i_{cref} and i_{sc}
- Fig. 10.14 DSTATCOM performance under linear load (a) Grid power (b) Load power (c)

Compensating power

- Fig. 10.15 DSTATCOM performance under unbalanced linear load (a)-(c) i_{sa} , i_{sb} , i_{sc} with v_{sab} (d)-(f) i_{La} , i_{Lb} , i_{Lc} with v_{sab} (g)-(i) i_{ca} , i_{cb} , i_{cc} along with v_{sab}
- Fig. 10.16 DSTATCOM performance under nonlinear balanced load (a)-(c) i_{sa} , i_{sb} , i_{sc} with v_{sab} (d)-(f) THD's of i_{sa} , i_{sb} , i_{sc} (g)-(i) i_{La} , i_{Lb} , i_{Lc} with v_{sab} (j)-(l) THD's of i_{La} , i_{Lb} , i_{Lc} (m)-(o) i_{ca} , i_{cb} , i_{cc} with v_{sab} (p)-(r) grid power, load power and compensating power
- Fig. 10.17 DSTATCOM performance under nonlinear unbalanced load (a)-(c) i_{sa} , i_{sb} , i_{sc} with v_{sab} (d)-(f) i_{La} , i_{Lb} , i_{Lc} with v_{sab} (g)-(i) i_{ca} , i_{cb} , i_{cc} with v_{sab}
- Fig. 10.18 DSTATCOM performance during the linear load disconnection in phase 'c' (a) v_{sab} , i_{sa} , i_{sb} and i_{sc} (b) v_{sab} , i_{La} , i_{Lb} and i_{Lc} (c) v_{sab} , i_{ca} , i_{cb} and i_{cc} (d) V_{dc} , i_{sc} , i_{Lc} and i_{cc}
- Fig. 10.19 DSTATCOM performance during the linear load injection in phase 'c' (a) v_{sab} , i_{sa} , i_{sb} and i_{sc} (b) v_{sab} , i_{La} , i_{Lb} and i_{Lc} (c) v_{sab} , i_{ca} , i_{cb} and i_{cc} (d) V_{dc} , i_{sc} , i_{Lc} and i_{cc}
- Fig. 10.20 DSTATCOM performance during the nonlinear load disconnection in phase 'c' (a) v_{sab} , i_{sa} , i_{sb} and i_{sc} (b) v_{sab} , i_{La} , i_{Lb} and i_{Lc} (c) v_{sab} , i_{ca} , i_{cb} and i_{cc} (d) V_{dc} , i_{sc} , i_{Lc} and i_{cc}
- Fig. 10.21 DSTATCOM performance during the nonlinear load injection in phase 'c' (a) v_{sab} , i_{sa} , i_{sb} and i_{sc} (b) v_{sab} , i_{La} , i_{Lb} and i_{Lc} (c) v_{sab} , i_{ca} , i_{cb} and i_{cc} (d) V_{dc} , i_{sc} , i_{Lc} and i_{cc}
- Fig. 11.1 Schematic of a DSTATCOM
- Fig. 11.2 Block diagram of HHT based control algorithm for a DSTATCOM
- Fig. 11.3 MATLAB model of DSTATCOM using HHT based control algorithm
- Fig. 11.4 HHT based control algorithm of DSTATCOM (a) unit templates estimation (b) extraction of fundamental component of load current (c) extraction of the active component of load current (d) extraction of average active component of load current (e) reference current estimation (f) generation of gate signals
- Fig. 11.5 EMD decomposition of the phase 'c' load current
- Fig. 11.6 Salient internal signals of the control algorithm for a nonlinear load with unbalancing in 'c' phase
- Fig. 11.7 System behaviour under balanced linear load with load unbalancing from time $t=0.2$ s to 0.3 s
- Fig. 11.8 System behaviour under balanced nonlinear load with unbalancing from time $t=0.2$ s to 0.3 s
- Fig. 11.9 Harmonic spectra of the proposed system at balanced load condition (a) v_{sab} (b) i_{sa} (c) i_{La}
- Fig. 11.10 Harmonic spectra of the proposed system at unbalanced load condition (a) v_{sab} (b) i_{sa} (c) i_{La}
- Fig. 11.11 Salient internal signals of the control algorithm during the nonlinear load disconnection (a) i_{Lc} , i_{fLc} , i_{AfLc} and I_{ApLg} (b), $\text{abs}(I_{pdc})$, I_{nApLg} , i_{cref} and i_{cc}
- Fig. 11.12 Salient internal signals of the control algorithm during the nonlinear load injection (a) i_{Lc} , i_{fLc} , i_{AfLc} and I_{ApLg} (b), $\text{abs}(I_{pdc})$, I_{nApLg} , i_{cref} and i_{sc}
- Fig. 11.13 DSTATCOM performance under linear balanced load (a) Grid power (b) Load power (c) Compensating power
- Fig. 11.14 DSTATCOM performance under linear unbalanced load (a)-(c) grid currents i_{sa} , i_{sb} , i_{sc} with v_{sab} (d)-(f) load current i_{La} , i_{Lb} , i_{Lc} with v_{sab} (g)-(i) compensating currents i_{sa} , i_{sb} , i_{sc} along with v_{sab}
- Fig. 11.15 DSTATCOM performance under nonlinear balanced load (a)-(c) grid currents i_{sa} , i_{sb} , i_{sc} along with grid voltage v_{sab} (d)-(f) THD's of i_{sa} , i_{sb} , i_{sc} (g)-(i) load currents i_{La} , i_{Lb} , i_{Lc} with v_{sab} (j)-(l) THD's of i_{La} , i_{Lb} , i_{Lc} (m)-(o) compensating currents i_{sa} , i_{sb} , i_{sc} along with v_{sab} (p)-(r) grid power, load power and

compensating power

- Fig. 11.16 DSTATCOM performance under nonlinear unbalanced load (a)-(c) grid currents i_{sa} , i_{sb} , i_{sc} with v_{sab} (d)-(f) load currents i_{La} , i_{Lb} , i_{Lc} with v_{sab} (g)-(i) compensating currents i_{ca} , i_{cb} , i_{cc} with v_{sab}
- Fig. 11.17 DSTATCOM performance during the linear load disconnection in phase 'c' (a) v_{sab} , i_{sa} , i_{sb} and i_{sc} (b) v_{sab} , i_{La} , i_{Lb} and i_{Lc} (c) v_{sab} , i_{ca} , i_{cb} and i_{cc} (d) V_{dc} , i_{sc} , i_{Lc} and i_{cc}
- Fig. 11.18 DSTATCOM performance during the linear load injection in phase 'c' (a) v_{sab} , i_{sa} , i_{sb} and i_{sc} (b) v_{sab} , i_{La} , i_{Lb} and i_{Lc} (c) v_{sab} , i_{ca} , i_{cb} and i_{cc} (d) V_{dc} , i_{sc} , i_{Lc} and i_{cc}
- Fig. 11.19 DSTATCOM performance during the nonlinear load disconnection in phase 'c' (a) v_{sab} , i_{sa} , i_{sb} and i_{sc} (b) v_{sab} , i_{La} , i_{Lb} and i_{Lc} (c) v_{sab} , i_{ca} , i_{cb} and i_{cc} (d) V_{dc} , i_{sc} , i_{Lc} and i_{cc}
- Fig. 11.20 DSTATCOM performance during the nonlinear load injection in phase 'c' (a) v_{sab} , i_{sa} , i_{sb} and i_{sc} (b) v_{sab} , i_{La} , i_{Lb} and i_{Lc} (c) v_{sab} , i_{ca} , i_{cb} and i_{cc} (d) V_{dc} , i_{sc} , i_{Lc} and i_{cc}

LIST OF TABLES

Table 3.1	Categories and typical characteristics of power system electromagnetic phenomena [IEEE std. 1159]
Table 3.2	Numerical modeling of single stage PQ disturbances
Table 3.3	Numerical modeling of multiple PQ disturbances
Table 3.4	Numerical modeling of multistage PQ disturbances
Table 5.1	Filter coefficients of various levels of CWT
Table 5.2	Frequency components of the various decomposition levels
Table 6.1	Confusion matrix for the disturbances of G_{21} group
Table 7.1	Confusion matrix for the PQ disturbances
Table 12.1	Comparison of S-transform performance with different classifiers
Table 12.2	Performance comparison of different techniques
Table 12.3	A comparison of computation burden
Table 12.4	A comparison of different algorithms with a nonlinear load in the balanced condition
Table 12.5	A comparison of different algorithms with a nonlinear load in the unbalanced condition

LIST OF ABBREVIATIONS

ACO	Ant Colony Optimization
AF	Active Filter
ANN	Artificial Neural Network
ASD	Adjustable Speed Drives
BNT	Balanced Neural Tree
CAIFI	Customer Average Interruption Frequency Index
CBEMA	Computer Business Equipment Manufacturer Association
CENELEC	European Committee for Electrotechnical Standardization
CF	Crest Factor
CPD	Custom Power Device
CWT	Complex Wavelet Transform
DAQ	Data Acquisition
DSTATCOM	Distribution Static Compensator
DVR	Dynamic Voltage Restorer
DWT	Discrete Wavelet Transform
EKF	Extended Kalman Filter
EMC	Electromagnetic Compatibility
EMD	Empirical Mode Decomposition
EN	European Norms
ES	Expert System
ESD	Electrostatic Discharge
FES	Fuzzy Expert System
FL	Fuzzy Rule
GA	Genetic Algorithm
HHT	Hilbert Haung Transform
HMM	Hidden Markov Model
HSA	Hilbert Spectral Analysis
IA	Instantaneous Amplitude
IEC	International Electrotechnical Commission
IEEE	Institute of Electrical and Electronics Engineers
IF	Instantaneous Frequency
IGBT	Insulated Gate Bipolar Transistor
IMF	Intrinsic Mode Function
IP	Instantaneous Phase
IRP	Instantaneous Reactive Power
ISC	Instantaneous Symmetrical Component

ITI	Information Technology Industry Council
ITIC	Information Technology Industry Council
KF	Kalman Filter
MAV	Moving Average Filter
MIF	Mean Instantaneous Frequency
ML	Maximum Likelihood
NEMP	Nuclear Electromagnetic Pulses
NI	National Instruments
NN	Neural Network
PCC	Point of Common Coupling
PLC	Programmable Logic Controller
PLL	Phase Locked Loop
PNN	Probabilistic Neural Network
PQ	Power Quality
PSO	Particle Swarm Optimization
RBF	Radial Basis Function
RMS	Root Mean Square
SAIDI	System Average Interruption Duration Index
SAIFI	System Average Interruption Frequency Index
SLG	Single Line to Ground
SNR	Signal to Noise Ratio
SRF	Synchronous Reference Frame
ST	Stockwell Transform
STFT	Short Time Fourier Transform
SVM	Support Vector Machine
THD	Total Harmonic Distortion
UPQC	Unified Power Quality Conditioner
VSC	Voltage Source Converter
WT	Wavelet Transform

LIST OF SYMBOLS

a	Overloading factor
C_{dc}	DC link Capacitances
C_f	Ripple filter capacitance
D	Second norm of the supply voltage
f_s	Sampling frequency
$i_{AfLa}, i_{AfLb}, i_{AfLc}$	Three phase active power components of load currents
i_{ApLg}	Average active power component of load currents
i_{ca}, i_{cb}, i_{cc}	Three phase instantaneous compensating currents
I_{crpp}	Current ripples
$i_{fLa}, i_{fLb}, i_{fLc}$	Three phase fundamental load components
i_{La}, i_{Lb}, i_{Lc}	Three phase instantaneous load currents
I_{nApLg}	Net active power component of supply currents
I_{peak}	Peak value of current
I_{pdc}	DC link voltage controller output
i_{sa}, i_{sb}, i_{sc}	Three phase instantaneous supply currents
$i_{aref}, i_{bref}, i_{cref}$	Three phase reference supply currents
K_i	Integral gain
K_p	Proportional gain
L_f	Interfacing inductance
m	Modulation index
p_{lavg}	Average active power of load
p_{loss}	Losses of DSTATCOM
p_s	Instantaneous three phase power of load
p_{st}	Total power from source
R_f	Ripple filter resistance
S_1 to S_6	Gating signals
T_s	Sampling time
u_{ap}, u_{bp}, u_{cp}	In-phase unit voltage templates
u_{aq}, u_{bq}, u_{cq}	Quadrature phase unit voltage templates
v_a, v_b, v_c	three phase instantaneous voltages
i_a, i_b, i_c	three phase instantaneous currents
v_a^+, v_b^+, v_c^+	Positive sequence components of the three phases
v_a^-, v_b^-, v_c^-	Negative sequence components of the three phases
v_a^0, v_b^0, v_c^0	Zero sequence components of the three phases
V_{dc}	DC link voltage
V_{dce}	DC link voltage error

V_{dc1}	Minimum DC link voltage
V_{LL}	Line to line voltage
V_p	Peak value of PCC voltage
v_p^+	Peak value of the positive sequence components
v_p^-	Peak value of the negative sequence components
v_{sa}, v_{sb}, v_{sc}	Three phase instantaneous supply voltages
$v_{sab}, v_{sbc}, v_{sca}$	Three phase instantaneous line voltages
V_{SW}	Voltage rating
Z_{sa}, Z_{sb}, Z_{sc}	Three phase source impedance
α	Fortescue operator
Φ	Phase angle
ε	Hysteresis band
ω	Angular frequency
τ	Shifting operator